

Article

Preparation of Peptide-Based Magnetogels for Removing Organic Dyes from Water

Farid Hajareh Haghighi ^{1,†} , Roya Binaymotlagh ^{1,†} , Paula Stefana Pintilei ¹, Laura Chronopoulou ^{1,2,*}  and Cleofe Palocci ^{1,2,*}

¹ Department of Chemistry, Sapienza University of Rome, Piazzale Aldo Moro 5, 00185 Rome, Italy

² Research Center for Applied Sciences to the Safeguard of Environment and Cultural Heritage (CIABC), Sapienza University of Rome, Piazzale Aldo Moro 5, 00185 Rome, Italy

* Correspondence: laura.chronopoulou@uniroma1.it (L.C.); cleofe.palocci@uniroma1.it (C.P.); Tel.: +39-06-4991-3317 (C.P.)

† These authors have contributed equally to this work.

Abstract: Water pollution by organic dyes represents a major health and environmental issue. Despite the fact that peptide-based hydrogels are considered to be optimal adsorbents for removing such contaminants, hydrogel systems often suffer from a lack of mechanical stability and complex recovery. Recently, we developed an enzymatic approach for the preparation of a new peptide-based magnetogel containing polyacrylic acid-modified γ -Fe₂O₃ nanoparticles (γ -Fe₂O₃NPs) that showed the promising ability to remove cationic metal ions from aqueous phases. In the present work, we tested the ability of the magnetogel formulation to remove three model organic dyes: methyl orange, methylene blue, and rhodamine 6G. Three different hydrogel-based systems were studied, including: (1) Fmoc-Phe₃ hydrogel; (2) γ -Fe₂O₃NPs dispersed in the peptide-based gel (Fe₂O₃NPs@gel); and (3) Fe₂O₃NPs@gel with the application of a magnetic field. The removal efficiencies of such adsorbents were evaluated using two different experimental set-ups, by placing the hydrogel sample inside cuvettes or, alternatively, by placing them inside syringes. The obtained peptide magnetogel formulation could represent a valuable and environmentally friendly alternative to currently employed adsorbents.

Keywords: magnetogels; magnetic γ -Fe₂O₃ nanoparticles; peptide-based hydrogels; water purification; methyl orange; methylene blue; rhodamine 6G



Citation: Hajareh Haghighi, F.; Binaymotlagh, R.; Pintilei, P.S.; Chronopoulou, L.; Palocci, C. Preparation of Peptide-Based Magnetogels for Removing Organic Dyes from Water. *Gels* **2024**, *10*, 287. <https://doi.org/10.3390/gels10050287>

Academic Editors: Shiyang Li, Zhenxing Fang and Kaiming Peng

Received: 28 March 2024

Revised: 18 April 2024

Accepted: 22 April 2024

Published: 24 April 2024



Copyright: © 2024 by the authors. Licensee MDPI, Basel, Switzerland. This article is an open access article distributed under the terms and conditions of the Creative Commons Attribution (CC BY) license (<https://creativecommons.org/licenses/by/4.0/>).

1. Introduction

Safe water is a global need for all aspects of life (e.g., household, industrial, and agricultural purposes) and, considering the current limitation of water resources, the importance of effective water recycling and purification is constantly growing [1]. Commonly used technologies for wastewater treatment are helpful but should be improved in terms of their economic feasibility, efficiency, and environmental footprint [2]. Due to the absence of adequate wastewater treatment methods, different dangerous materials constantly enter natural water resources [3]. Every year, tons of chemically stable synthetic dyes are wasted from the pharmaceutical [4,5], garment [6], textile [7], leather, ink, paper [8], and plastic industries [9], negatively affecting aquatic life and also threatening human health, as many of these chemicals are highly hazardous and have been classified as mutagenic, carcinogenic, or genotoxic [10]. Furthermore, these water contaminants decrease sunlight penetration into bodies of water, which influences photosynthetic processes and affects aquatic flora and fauna [11]. In particular, sunlight plays a crucial role in the photosynthesis of aquatic plants. It provides the energy needed for the conversion of inorganic carbon to organic carbon compounds, which is the fundamental biological process on Earth. Synthetic dyes such as methylene blue (MB), rhodamine 6G (Rh6G) (model cationic dyes), and methyl orange

(MO) (a model anionic dye) cause several health disorders like respiratory tract infections, skin disease, and eye irritation, so their removal from water resources is necessary [12].

There are standard methods for wastewater treatment, including chemical precipitation, adsorption, ion exchange, electrochemical separation, and coagulation-flocculation methods. Nonetheless, all of these methods have some drawbacks, e.g., high energy consumption, partial contaminant elimination, high operation costs, and the production of toxic sludges [13]. Today, the removal of contaminants from wastewater is considered a crucial step towards achieving sustainable development. Among the approaches listed [14], adsorption is still the most commonly used method, and an ideal adsorbent removes most pollutants and can be recovered easily using cost-effective methods like electrochemical or solvent treatments [15,16]. However, common commercial adsorbents such as biochar, zeolites, and activated carbon pose a high risk of water contamination by themselves.

Recently, hydrogel nanohybrids have become increasingly used in numerous adsorption-based water treatment applications [17]: generally, a polymer forms a hydrophilic porous network and nanomaterials are used as modifiers to enhance the adsorption properties [18]. For water remediation, the possibility of using biocompatible materials is very important. Peptide hydrogels can be considered as promising candidates to decrease the self-contamination risk of adsorbent systems [19]. Compared with commercially available adsorbents, these hydrogels benefit from being porous and highly hydrophilic, as well as from possessing large surface areas and numerous functional groups. In particular, short self-assembling peptides are an interesting class of biocompatible and biodegradable hydrogel-forming materials. Their synthesis is generally simple and scalable. Moreover, both the properties and self-assembly of peptides can be tuned by altering the peptide sequence [20].

Magnetic nanoparticles (NPs) can be incorporated into hydrogels to provide a magnetic property to the resulting hybrid system. Among magnetic nanostructures, magnetite (Fe_3O_4) and maghemite ($\gamma\text{-Fe}_2\text{O}_3$) NPs have been extensively used for environmental applications because of their biocompatibility, well-assessed synthesis methods, and on/off superparamagnetic properties [21]. Although $\gamma\text{-Fe}_2\text{O}_3$ NPs show a slightly smaller magnetic moment than Fe_3O_4 NPs, they are more stable in air [22], and more reliable for practical applications. To date, various nanohybrid-based $\gamma\text{-Fe}_2\text{O}_3$ NPs have been used as adsorbents to remove several organic dyes (e.g., MO, rose bengal, MB, brilliant cresyl blue, Congo red, thionine, and Janus green B) from aqueous solutions with significant adsorption efficiencies. Aside from the numerous advantages of peptide-based hydrogel nanohybrids, their poor mechanical properties and low elasticity are their two main limitations in water remediation applications; however, these drawbacks may be overcome by using appropriate cross-linkers.

In a recent work [23], we reported the preparation of a new peptide composite magnetogel made of a Fmoc-Phe₃ hydrogel matrix containing $\gamma\text{-Fe}_2\text{O}_3$ -polyacrylic acid (PAA) NPs ($\gamma\text{-Fe}_2\text{O}_3$ NPs) and its application for removing Cr(III), Ni(II), and Co(II) from water, demonstrating that both the native hydrogel as well as the magnetogel can effectively eliminate all the examined metal ions from water. Moreover, thanks to the presence of $\gamma\text{-Fe}_2\text{O}_3$ NPs, the efficiency of this system can be promoted by the application of a magnetic field. In the present study, we tested the ability of the magnetogel formulation to remove three model dyes: MO, MB, and Rh6G. On this basis, three different hydrogel-based systems, including (1) Fmoc-Phe₃ hydrogel (gel); (2) $\gamma\text{-Fe}_2\text{O}_3$ NPs loaded in the hydrogel ($\gamma\text{-Fe}_2\text{O}_3$ NPs@gel); and (3) $\gamma\text{-Fe}_2\text{O}_3$ NPs@gel in the presence of an external magnetic field ($\gamma\text{-Fe}_2\text{O}_3$ NPs@gel + mf), were studied. The removal efficiency of these gels was evaluated using two experimental set-ups, by placing hydrogel samples: (1) inside cuvettes or (2) inside syringes.

2. Results and Discussion

2.1. Preparation of γ -Fe₂O₃NPs and Magnetogels

The magnetogel nanohybrids were synthesized in two steps, as described in our previous publication [23]. Firstly, PAA-stabilized γ -Fe₂O₃NPs were prepared by a co-precipitation method to obtain small and colloiddally stable NPs. Co-precipitation is an uncomplicated and cost-effective way to prepare γ -Fe₂O₃NPs, and involves starting from aqueous solutions of Fe(II) and Fe(III) and adding a base as a precipitating agent. This method requires mild temperatures and no organic solvents or toxic precursors, and allows for the preparation of large amounts of NPs. Also, thanks to its simpleness, reliability, and environmentally friendly conditions, it can be adjusted and scaled up to an industrial scale.

For the magnetogel synthesis, γ -Fe₂O₃NPs were suspended in an aqueous phase containing the hydrogel precursors and the gelation process was carried out. The main advantage of such a blending method is its simplicity; however γ -Fe₂O₃NPs must be stabilized (i.e., with PAA) to prevent their heterogeneous distribution within the hydrogel network. The hydrogel formation was conducted using a biotechnological approach that employs a microbial lipase to catalyze the formation of the Fmoc-Phe₃ hydrogelator, as previously reported [24]. The resulting magnetogel was characterized in a previous work through FT-IR, Raman, and XPS experiments [23].

2.2. Rheology and Swelling Ability Studies

Rheological studies were conducted to unravel the influence of the modifiers used on the tensile strength of peptide hydrogels. The presence of γ -Fe₂O₃NPs was able to enhance the rheological properties of the hydrogel, as previously reported (Figure 1a).

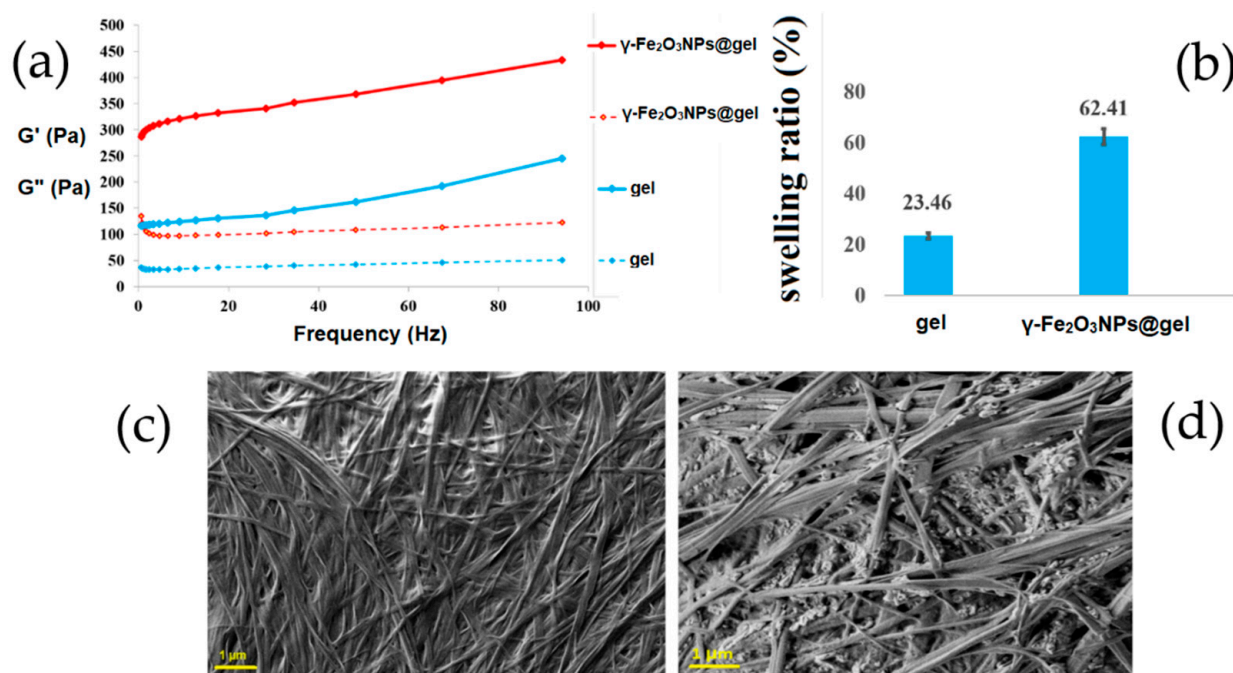


Figure 1. (a) Frequency sweep of the gel and γ -Fe₂O₃NPs@gel; (b) swelling abilities of the gel and γ -Fe₂O₃NPs@gel; SEM images of: (c) the gel and (d) γ -Fe₂O₃NPs@gel.

After the addition of γ -Fe₂O₃NPs to the pristine hydrogel, its swelling ability increased up to \approx 62%, which may be related to the presence of NPs that provide porosity inside the hydrogel, increasing its swelling properties (Figure 1b).

2.3. SEM Experiments

SEM was employed to investigate the morphology of the pristine gel as well as that of the magnetogel. Figure 1c shows the typical fibrillary structure of the pristine hydrogel.

The fibrils are several micrometers long while their width is between 100 and 150 nm. The addition of magnetic NPs to the gel did not seem to have any significant effect on its fibrillary structure (Figure 1d). On the basis of SEM experiments, the average size of $\gamma\text{-Fe}_2\text{O}_3$ NPs was determined to be in a range between 15 and 60 nm.

2.4. Removal Studies of MB, Rh6G and MO from Water

Two different experimental set-ups were developed for the removal of MB, Rh6G, and MO by using different hydrogel samples (Figure 2). In the first set of experiments, the gel samples were prepared inside cuvettes, then the aqueous dye solution was placed on top of them. With this configuration, the dyes diffuse into the gel matrix by gravity (without the need to apply any external forces). In the other set of experiments, the gel samples were prepared inside syringes. In the removal experiments, the dye solutions were allowed to flow inside the syringes, placed vertically, either by gravity or by applying an external force. Therefore, in this set-up, the dyes pass through the gel matrix and exit from the lower inlet of the syringe.

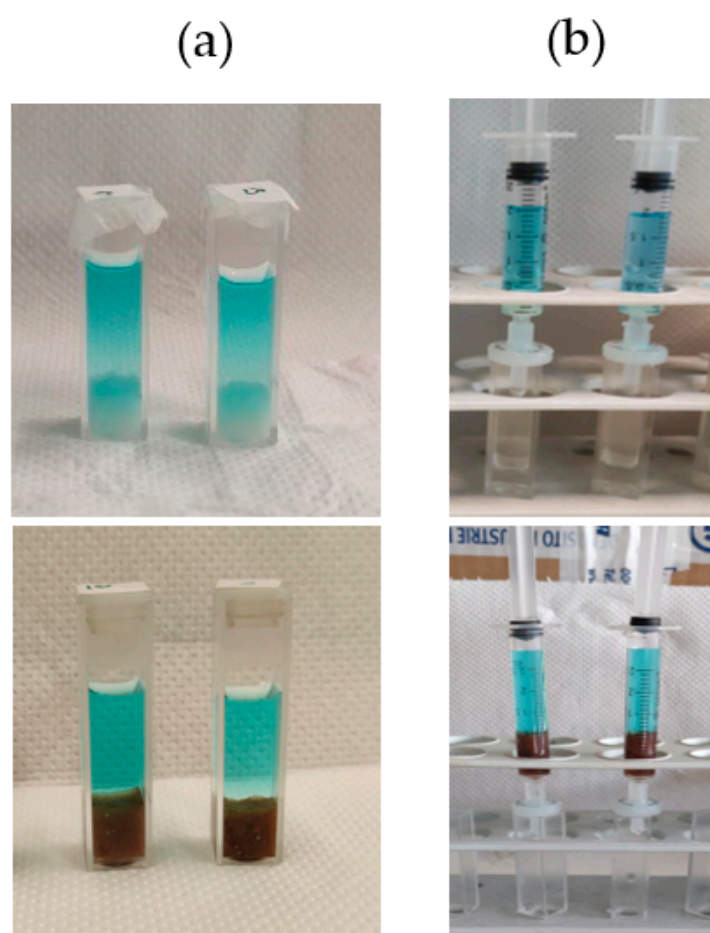


Figure 2. The two different set-ups used for the removal studies of organic dyes from water: (a) employing cuvettes and (b) employing syringes.

2.4.1. Experimental Set-Up Employing Cuvettes

MB has a heterocyclic aromatic structure (Figure 3) with characteristic absorbance peaks at 293 and 664 nm, related to $\pi-\pi^*$ and $n-\pi^*$ transitions, respectively [25]. The visible absorption (664 nm) was monitored during the MB removal studies. Regarding Rh6G, it contains a xanthene moiety that is responsible for its $\pi-\pi^*$ absorption at visible wavelengths [26]. The visible absorption at 527 nm was monitored to evaluate the Rh6G removal by the adsorbents. The anionic dye MO has a strong absorption at around 500 nm, which was selected for the adsorption experiments.

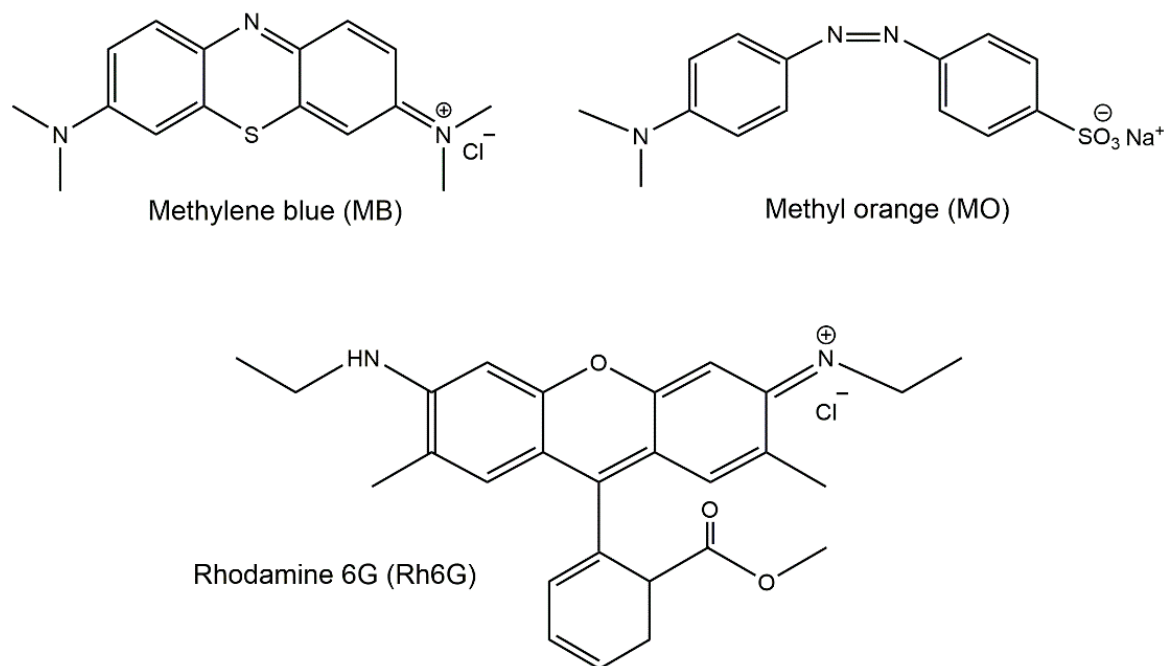


Figure 3. Chemical structures of methylene blue (MB), rhodamine 6G (Rh6G) (model cationic dyes), and methyl orange (MO) (model anionic dye).

Three different adsorbents were used to remove the three organic dyes described above from aqueous solutions: the native gel, γ -Fe₂O₃NPs@gel, and γ -Fe₂O₃NPs@gel + mf (mf: external magnetic field).

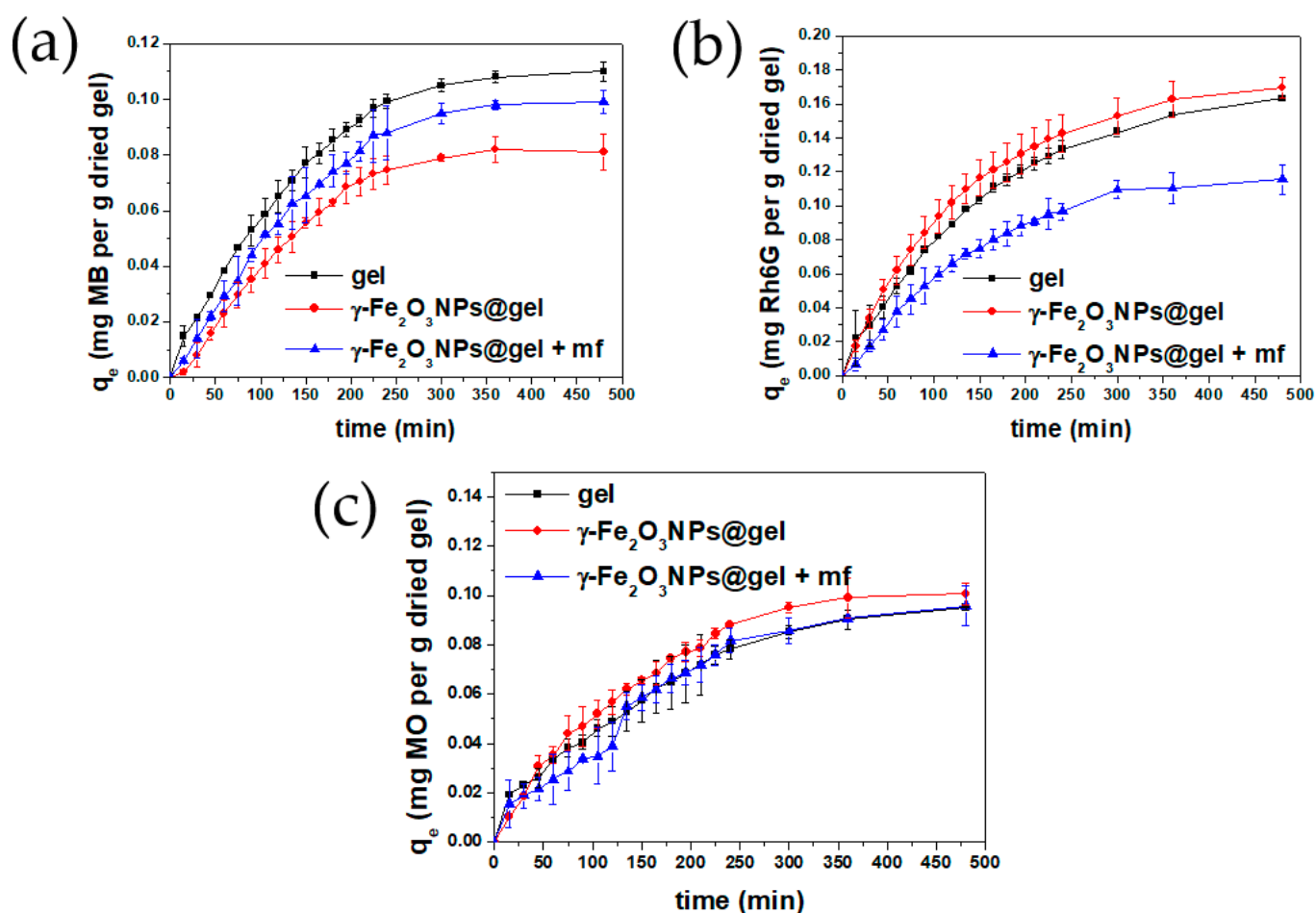
In particular, the adsorption abilities of these materials were evaluated at different contact times with the solution of the selected dye and expressed as q_t (mg of dye absorbed by 1 g of dry hydrogel). The evolution of the q_t values as a function of time for each dye + adsorbent system is reported in the plots in Figure 4a–c, for contact times ranging from 0 to 480 min. Also, Tables 1 and 2 show the removal efficiencies/capacities and calculated kinetic parameters of the three adsorbent systems for the three dyes, respectively.

Table 1. Removal efficiencies and capacities (q_e) of different hydrogel systems for MB, Rh6G, and MO.

	Adsorbent	Removal Efficiency% (RE%)	q_e (mg g ⁻¹)
MB	gel	30.8 ± 1	0.11 ± 0.0
	γ -Fe ₂ O ₃ NPs@gel	22.7 ± 2	0.08 ± 0.0
	γ -Fe ₂ O ₃ NPs@gel + mf	27.7 ± 1	0.09 ± 0.0
Rh6G	gel	45.7 ± 1	0.16 ± 0.0
	γ -Fe ₂ O ₃ NPs@gel	47.5 ± 1	0.17 ± 0.0
	γ -Fe ₂ O ₃ NPs@gel + mf	32.4 ± 2	0.11 ± 0.0
MO	gel	13.3 ± 1	0.09 ± 0.0
	γ -Fe ₂ O ₃ NPs@gel	14.1 ± 0	0.10 ± 0.0
	γ -Fe ₂ O ₃ NPs@gel + mf	13.4 ± 0	0.09 ± 0.0

Table 2. Kinetic data obtained from pseudo-first- and pseudo-second-order models for different hydrogel systems and MB, Rh6G, or MO at RT.

	Adsorbent	Pseudo-First Order			Pseudo-Second Order		
		k_1 (min^{-1})	q_e (mg g^{-1})	R^2	k_2 ($\text{g mg}^{-1} \text{min}^{-1}$)	q_e (mg g^{-1})	R^2
MB	gel	0.011	0.14	0.9715	0.037	0.16	0.9713
	$\gamma\text{-Fe}_2\text{O}_3\text{NPs@gel}$	0.012	0.12	0.9493	0.0028	0.35	0.1329
	$\gamma\text{-Fe}_2\text{O}_3\text{NPs@gel} + \text{mf}$	0.011	0.15	0.9323	0.017	0.18	0.8257
Rh6G	gel	0.0074	0.17	0.992	0.023	0.23	0.9822
	$\gamma\text{-Fe}_2\text{O}_3\text{NPs@gel}$	0.0080	0.18	0.9881	0.026	0.23	0.9921
	$\gamma\text{-Fe}_2\text{O}_3\text{NPs@gel} + \text{mf}$	0.0089	0.14	0.9696	0.018	0.20	0.8597
MO	gel	0.0069	0.10	0.9712	0.048	0.13	0.954
	$\gamma\text{-Fe}_2\text{O}_3\text{NPs@gel}$	0.010	0.13	0.9328	0.037	0.15	0.9832
	$\gamma\text{-Fe}_2\text{O}_3\text{NPs@gel} + \text{mf}$	0.0080	0.11	0.9638	0.024	0.15	0.8149

**Figure 4.** Adsorption capacities (q_t , mg/g) of the native gel, $\gamma\text{-Fe}_2\text{O}_3\text{NPs@gel}$, and $\gamma\text{-Fe}_2\text{O}_3\text{NPs@gel} + \text{mf}$, versus time for MB (a), Rh6G (b), and MO (c).

The results obtained with this experimental set-up show that the magnetic NPs change the adsorption properties of the pristine gels and, also, that the addition of an external magnetic field additionally modifies the adsorbing character of the gels. Over the whole removal process for the three examined systems, no significant changes were detected in the

maximum wavelengths of the dyes and, as can be seen in Figure 4a–c, the dye adsorption decreased with time. This general feature, observed for all dyes and adsorbents, is probably linked to the progressive saturation of the adsorbing sites of the gels over time, which eventually reaches equilibrium after approximately 400 min.

Figure 4a shows that the q_t values for MB follow the trend gel > $\gamma\text{-Fe}_2\text{O}_3\text{NPs@gel} + \text{mf}$ > $\gamma\text{-Fe}_2\text{O}_3\text{NPs@gel}$, which is different from those observed for Rh6G and MO, where $\gamma\text{-Fe}_2\text{O}_3\text{NPs@gel}$ exhibits the best performance in terms of dye removal (Figure 4b,c). Such a difference may be ascribed to the different structures of the dyes, which affect the gel–dye interaction at the molecular level.

Another result worth mentioning is the changes in removal efficiencies (RE%) and final adsorption capacities for different systems, summarized in Table 1. For MB, the results show that the removal efficiencies of $\gamma\text{-Fe}_2\text{O}_3\text{NPs@gel}$ and $\gamma\text{-Fe}_2\text{O}_3\text{NPs@gel} + \text{mf}$ are decreased by 26.3% and 10.1%, respectively, in comparison with the native gel. For Rh6G, both magnetogels and pristine gels show similar RE% values, and the combination of magnetogels with the application of a magnetic field significantly drops the adsorption efficiency by 29.1%. For MO, the magnetogel shows the highest RE% value, while the interaction of magnetogels with the magnetic field increases the dye removal by 16.7%.

Regarding the different effect of $\gamma\text{-Fe}_2\text{O}_3\text{NPs}$ on dye adsorption, it is in good agreement with data from the literature on magnetogels [27,28] and is due to the ability of NPs embedded in hydrogels to affect both the cross-linking degree and porosity of the gels, influencing the surface channels and, therefore, the entry, exit, and adsorption of molecules [29]. Also, the application of an external magnetic field can further change the adsorption, because magnetogels are able to exert an on/off effect on the hydrogel pores [30]. The magnetic dipole-dipole orientation of $\gamma\text{-Fe}_2\text{O}_3\text{NPs}$ towards the external magnetic field is able to affect the swelling and shrinking of $\gamma\text{-Fe}_2\text{O}_3\text{NPs@gels}$ [31], most probably affecting the permeability of dyes into the gel network [32,33].

As is well known, the study of adsorption kinetics is able to provide information on the nature of the adsorption (e.g., physisorption or chemisorption) [34]. In this study, we used pseudo-first- and pseudo-second-order kinetic models [22], as described in the Supplementary Materials. The obtained kinetic parameters are summarized in Table 2, where the best correlations (in terms of R^2) of MB and Rh6G studies were mainly obtained when using the pseudo-first-order kinetic model, although not for $\gamma\text{-Fe}_2\text{O}_3\text{NPs@gel}$ (Rh6G) studies. For this system, the equilibrium adsorption capacity, q_e , obtained from the pseudo-first-order relation was more similar to the experimental values reported in Figure 4 and Table 1, suggesting that the adsorption of Rh6G onto these adsorbents mainly occurs through physisorption. MB and Rh6G dyes possess cationic imine and amine groups that can favor their adsorption on the hydrogels, thanks to different electrostatic interactions that may occur, such as that between the positively charged imine nitrogen of the dyes and the negatively charged hydroxyl groups of the hydrogel. Moreover, H-bonding interactions among the amine group of the dyes and the hydroxyl groups of the hydrogels may be established [35]. Returning to the possible pseudo-second-order mechanism estimated for $\gamma\text{-Fe}_2\text{O}_3\text{NPs@gel}$ (Rh6G), it is attributed to chemisorption, which may depend on the chelation between the carboxyl and amine groups of the gels ($-\text{NH}$, $-\text{OH}$, and $-\text{COOH}$) and the lone pair electrons of the dye molecules [36–41]. Conversely, to these cationic dyes, MO (as an anionic dye) shows much lower RE% and q_e values, which may be related to its negative charge significantly limiting its electrostatic interaction with the gels, even though it was used at higher initial concentrations (10 ppm) than MB and Rh6G (5 ppm). For MO, two adsorbents show physisorption (gel and $\gamma\text{-Fe}_2\text{O}_3\text{NPs@gel} + \text{mf}$), controlled by physical forces like dipole–dipole interactions, hydrogen bonds, van der Waals forces, and hydrophobic interactions. Based on these results, the prepared adsorbent is more suitable for the removal of cationic dyes, rather than anionic ones.

2.4.2. Experimental Set-Up Employing Syringes

The absorbing abilities of native gel, $\gamma\text{-Fe}_2\text{O}_3\text{NPs@gel}$, and $\gamma\text{-Fe}_2\text{O}_3\text{NPs@gel} + \text{mf}$ towards the selected dyes were tested with the experimental set-up employing syringes (Figure 5). Three different conditions were used, including (1) gravitational passage of the dye through the gels inside the syringe (Figure S2a); (2) gravitational passage with the application of filters attached to the outlet of the syringe (Figure S2b); and (3) the application of a constant pressure to increase the flow rate of the dye inside the syringe, combined with the use of a filter at the outlet of the syringe (Figure S2c). In terms of time and reproducibility, the third set-up was selected as the optimized condition for studying the absorbing abilities of the gels. It must be taken into account that the filters absorb part of the dye; therefore, this filter absorption was quantified for each dye and then subtracted from the amount of dye removed by each hydrogel system (see Figures S3–S6).

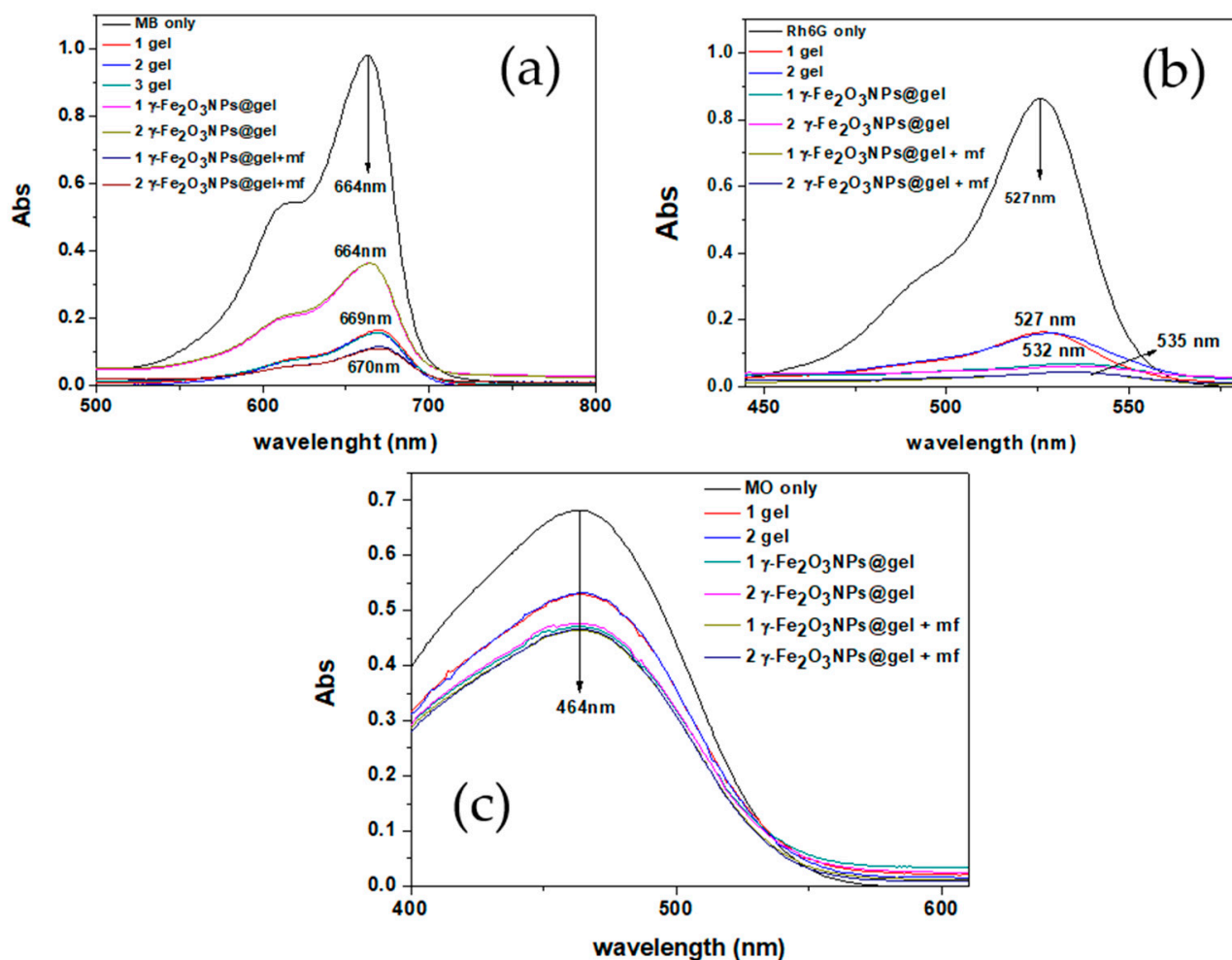


Figure 5. Absorbing abilities of gel, $\gamma\text{-Fe}_2\text{O}_3\text{NPs@gel}$, and $\gamma\text{-Fe}_2\text{O}_3\text{NPs@gel} + \text{mf}$ for the removal of (a) MB ($C_0 = 5$ ppm, pH = 7.4, 1 mg of adsorbent, flow rate = 0.2 mL/min); (b) Rh6G ($C_0 = 5$ ppm, pH = 7.2, 1 mg of adsorbent, flow rate = 0.2 mL/min); (c) MO ($C_0 = 10$ ppm, pH = 7.5, 1 mg of adsorbent, flow rate = 0.2 mL/min).

For the cationic dyes, MB and Rh6G, significant adsorptions (>60%) were observed for all adsorbents (gel, $\gamma\text{-Fe}_2\text{O}_3\text{NPs@gel}$ and $\gamma\text{-Fe}_2\text{O}_3\text{NPs@gel} + \text{mf}$) (Table 3). For MB, the pristine gel showed a 20.3% higher RE% than the magnetogel; however, when the external magnet was used, the $\gamma\text{-Fe}_2\text{O}_3\text{NPs@gel} + \text{mf}$ system demonstrated a 4.5% higher RE% than the native hydrogel. For both the $\gamma\text{-Fe}_2\text{O}_3\text{NPs@gel} + \text{mf}$ and pristine gel systems, a red-shift was also detected, which may be attributed to the decrease in the dye's concentration after passing through the gels. The UV-Vis spectrum of the initial MB solution shows a

monomeric structure for the dye that can exist in two monomeric mesomers (I and II), based on data from the literature (see Figure 6) [42].

Table 3. Adsorption efficiencies of different hydrogel systems for the removal of MB, Rh6G, or MO from an aqueous phase using the experimental set-up employing syringes.

	Adsorbent	RE% of Cuvette Set-Up	RE% of Syringe Set-Up
MB	gel	30.8 ± 1	80.4 ± 1
	γ -Fe ₂ O ₃ NPs@gel	22.7 ± 2	60.1 ± 2
	γ -Fe ₂ O ₃ NPs@gel + mf	27.7 ± 1	84.9 ± 0
R6G	gel	45.7 ± 1	83.2 ± 1
	γ -Fe ₂ O ₃ NPs@gel	47.5 ± 1	95.0 ± 0
	γ -Fe ₂ O ₃ NPs@gel + mf	32.4 ± 2	97.6 ± 0
MO	gel	13.3 ± 1	21.8 ± 7
	γ -Fe ₂ O ₃ NPs@gel	14.1 ± 0	30.0 ± 6
	γ -Fe ₂ O ₃ NPs@gel + mf	13.4 ± 0	31.3 ± 6

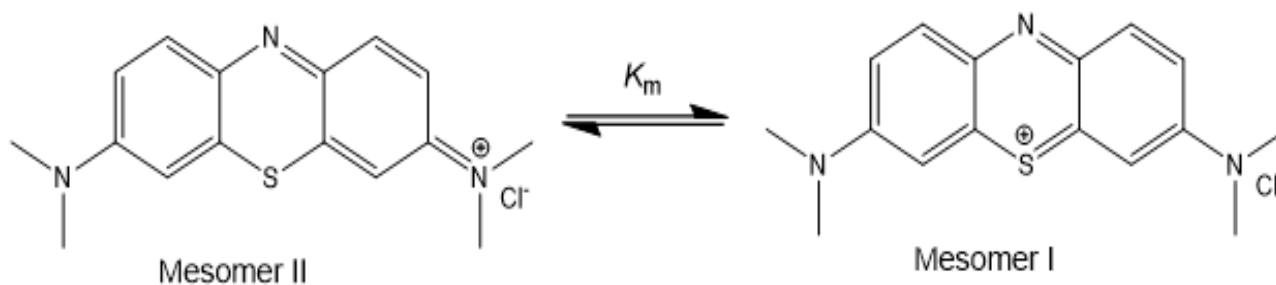


Figure 6. Alternative mesomeric structures for MB [41].

Based on Fernández-Pérez's work on the mesomeric structure of MB in water, we propose that, after the removal of the dye by the native gel or γ -Fe₂O₃NPs@gel + mf, the purified solutions contain the mesomeric II structure of MB, which has different UV-Vis adsorption with the observed red-shift, compared to the initial MB solution.

For Rh6G, more than 95% of the dye was removed by both γ -Fe₂O₃NPs@gel and γ -Fe₂O₃NPs@gel + mf and, for the observed red-shift of the purified solutions, a monomer/dimer change in Rh6G may be proposed. In fact, the initial solution of Rh6G shows a combination of monomer/dimer species for the dye. After dilution, the concentration of monomers becomes significant and a spectral change is observed. Another important factor is the possible release of ions (e.g., Na⁺, Cl⁻) from the hydrogel matrix to the filtered solutions, which can also affect the spectral pattern on the dyes.

Conversely, regarding the cationic dyes, for MO, no significant spectral changes were detected after the filtration; the RE% values for MO are much lower (20–30%) compared to those for MB and Rh6G, probably due to the different charges in the dyes. Regarding the amount of MO adsorbed by the three hydrogel systems, γ -Fe₂O₃NPs@gel and γ -Fe₂O₃NPs@gel + mf show the same adsorption efficiencies (approximately 30%), compared to the lower amounts observed for the pristine gel (approximately 20%).

In Table 4, the adsorption capacities of γ -Fe₂O₃NPs@gel + mf (in the experimental set-up employing syringes) towards cationic dyes were compared with those of similar adsorbents described in the literature. The observed lower adsorption capacities for the magnetogels described in this study may be improved by modifying the formulation of the magnetogels, e.g., using cross-linkers that could also improve the mechanical stability of the magnetogels and, therefore, their reusability as adsorbents.

Table 4. Comparison of the adsorption capacities of γ -Fe₂O₃NPs@gel + mf with similar adsorbents for the removal of cationic dyes.

Adsorbent	Cationic Dyes	C ₀ (mg mL ⁻¹)	Adsorption Capacities of Syringe Set-Up (mg g ⁻¹)	Reference
γ -Fe ₂ O ₃ NPs@gel + mf	MB	0.005	0.9	this work
γ -Fe ₂ O ₃ NPs@gel + mf	Rh6G	0.005	1.1	this work
poly(acrylic acid-acrylamide-butyl methacrylate) magnetic hydrogel	MB	50–100	12.6	[43]
Fe ₃ O ₄ /poly(2-hydroxyethyl methacrylate-co-itaconic acid) magnetic hydrogels	MB	0.05–0.2	174.9	[44]
poly(2-(2-methoxyethoxy) ethyl methacrylate-co-oligo (ethylene glycol) methacrylate-co-acrylic acid) (PMOA) hydrogel-magnetic attapulgitite/Fe ₃ O ₄	RhB (rhodamine B)	0.001	1.65	[45]

By comparing the two experimental setups (cuvettes and syringes, see Table 3), it can be seen that the adsorption using cuvettes is much lower, as it occurs only at the interface between the gel and solution, while in the case of syringes, the solution passes through the mass of the gel, allowing a greater interaction with it and, consequently, a greater adsorption of the dyes. More importantly, in each methodology, the trends of the RE% values of the adsorbents (Figures S7–S9) are changed.

3. Conclusions

Composite hydrogels have interesting adsorption properties and, in this study, we reported that the incorporation of magnetic NPs inside peptide-based hydrogels can be a valuable approach to additionally increase the adsorption capacities of hydrogels. In particular, the γ -Fe₂O₃NPs@gel + mf system was able to absorb up to 84% of MB and 97% of Rh6G from aqueous solutions containing 5 ppm of the dyes. However, for the anionic dye MO, the gels showed much lower adsorption capacities (lower than 30%) due to the dominant electrostatic repulsions between MO and the gel components.

The kinetic models of the cationic dyes mainly showed a physisorption mechanism for these adsorbents, while, for MO, both chemisorption and physisorption were observed, depending on the type of adsorbent. The results presented here support the application of peptide-based magnetogels in wastewater treatment. Future work should focus on scaling up materials' preparation and testing them in practical scenarios.

4. Materials and Methods

4.1. Materials

L-Phenylalanyl-L-phenylalanine and *N*-(9-Fluorenylmethoxycarbonyl)-L-phenylalanine were obtained from Bachem GmbH (Weil am Rhein, Germany). All other chemicals, including FeCl₂·4H₂O, FeCl₃, and *Pseudomonas fluorescens* Lipase ($\geq 20,000$ U/mg) were purchased from Sigma-Aldrich (Saint Louis, MO, USA). All chemicals were employed without further purification. Ultra-pure water was prepared with a Zeneer Power I Scholar-UV (Full Tech Instruments, Rome, Italy) apparatus. The external magnetic field was generated by using a neodymium-based magnet (volume = 39.270 cm³, magnetization quality = N5, magnetic strength = 1.42–1.47 T).

4.2. Synthesis of γ -Fe₂O₃NPs@gel Magnetogels

Magnetogels were prepared with a two-step procedure, first preparing PAA-stabilized γ -Fe₂O₃NPs and then dispersing them in the aqueous solution of hydrogel precursors before gelation. The details of the synthetic procedures have been described previously [23].

4.3. SEM Analysis

SEM analyses were conducted with an Auriga field emission scanning electron microscope (Zeiss, Oberkochen, Germany), as previously described [23].

4.4. Rheological Measurements

The dynamo-mechanical analyses (mechanical spectroscopy) were studied for four samples including hydrogel and three magnetogels containing different concentrations of NPs. Rheological studies were carried out with an MCR 302 rotational rheometer (Anton Paar, Turin, Italy), as previously described [23].

4.5. Swelling Ability

Three mL of phosphate buffer solution (PBS, pH = 7.4) was placed on top of each hydrogel sample, followed by incubation at 30 °C in a thermostatic bath. After 24 h, the supernatants were removed and the samples were freeze-dried. The swelling degree was evaluated by using the following equation:

$$q = (W_s - W_d)/W_d \quad (1)$$

where q = swelling degree, W_s = weight of the gel after PBS removal, and W_d = weight of the freeze-dried gel.

4.6. Adsorption Experiments

For the cuvette experiments, gel and magnetogel samples were prepared in glass cuvettes. Then, 2 mL of aqueous dye solution (MB, Rh6G or MO) was cast on top of the gels. The concentration of MB and Rh6G was 5 ppm, while the MO concentration was 10 ppm.

UV-Vis spectroscopy was employed to monitor the absorbances of the solutions every 15 min. The removal efficiencies (RE) were calculated using Equation (2):

$$RE(\%) = (C_0 - C_f)/C_0 \times 100 \quad (2)$$

where C_0 = initial dye concentration, C_f = dye concentration in the eluted solution.

Calibration curves were prepared for each dye and used for the calculations. The adsorption capacities (q_t , mg g⁻¹) of the adsorbents were calculated using Equation (3) [23]:

$$q_t = (C_0 - C_t)/m \times V \quad (3)$$

in which m (g) is the dried hydrogel mass, C_0 and C_t (mg L⁻¹) are the initial and equilibrium dye concentrations, and V (L) is the solution volume, respectively.

The kinetics of dye adsorption were analyzed with non-linear pseudo-first- and pseudo-second-order kinetic models (Equations (4) and (5)) [22].

$$\log(q_e - q_t) = \log q_e - k_1 t/2.303 \quad (4)$$

$$t/q_t = 1/k_2 q_e^2 + t/q_e \quad (5)$$

Supplementary Materials: The following supporting information can be downloaded at: <https://www.mdpi.com/article/10.3390/gels10050287/s1>, Materials and Methods; Figure S1: (a) Calibration curve of methylene blue (MB); (b) calibration curve of rhodamine 6G (R6G); (c) calibration curve of methyl orange (MO).; Figure S2: (a) Gravitational passage of MB through the gels inside the syringe; (b) gravitational passages with applying the filter in the outlet of the syringe; (c) gravitational passage with applying the filter and a constant pressure to increase the flow rate of the dye inside the syringe.; Figure S3: (a) Absorption of MB by the filter for different cycles; (b) amount of MB adsorbed by the filter in each cycle; (c) visual observation of the MB adsorption by the filter.; Figure S4: (a) Absorption of Rh6G by the filter for different cycles; (b) amount of Rh6G adsorbed by the filter in each cycle;

(c) visual observation of the Rh6G adsorption by the filter.; Figure S5: (a) Absorption of MO by the filter for different cycles; (b) amount of MO adsorbed by the filter in each cycle; (c) visual observation of the MO adsorption by the filter. Figure S6: (a) Separation of the dyes by gel, γ -Fe₂O₃NPs@gel, and (γ -Fe₂O₃NPs@gel + mf) using the syringe with filter and external pressure for (a) MB; (b) Rh6G; (c) and MO.; Figure S7: Comparison of the cuvette and syringe methodology for the MB adsorption by (a) gel, (b) γ -Fe₂O₃NPs@gel, and (c) γ -Fe₂O₃NPs@gel + mf.; Figure S8: Comparison of the cuvette and syringe methodology for the Rh6G adsorption by (a) gel, (b) γ -Fe₂O₃NPs@gel, and (c) γ -Fe₂O₃NPs@gel + mf.; Figure S9: Comparison of the cuvette and syringe methodology for the MO adsorption MO by (a) gel, (b) γ -Fe₂O₃NPs@gel, and (c) γ -Fe₂O₃NPs@gel + mf.

Author Contributions: Conceptualization: F.H.H. and R.B.; Methodology: L.C., R.B. and F.H.H.; Investigation: P.S.P., F.H.H. and R.B.; Data curation: L.C. and C.P.; Writing—original draft preparation: F.H.H. and R.B.; Writing—review and editing, L.C. and C.P. All authors have read and agreed to the published version of the manuscript.

Funding: This research received no external funding.

Institutional Review Board Statement: Not applicable.

Informed Consent Statement: Not applicable.

Data Availability Statement: The data presented in this study are available in the article.

Conflicts of Interest: The authors declare no conflicts of interest.

References

1. Waghchaure, R.H.; Adole, V.A.; Jagdale, B.S. Photocatalytic Degradation of Methylene Blue, Rhodamine B, Methyl Orange and Eriochrome Black T Dyes by Modified ZnO Nanocatalysts: A Concise Review. *Inorg. Chem. Commun.* **2022**, *143*, 109764. [[CrossRef](#)]
2. Salahuddin, B.; Aziz, S.; Gao, S.; Hossain, M.S.A.; Billah, M.; Zhu, Z.; Amiralian, N. Magnetic Hydrogel Composite for Wastewater Treatment. *Polymers* **2022**, *14*, 5074. [[CrossRef](#)]
3. Chiam, S.L.; Pung, S.Y.; Yeoh, F.Y. Recent Developments in MnO₂-Based Photocatalysts for Organic Dye Removal: A Review. *Environ. Sci. Pollut. Res.* **2020**, *27*, 5759–5778. [[CrossRef](#)]
4. Domacena, A.M.G.; Aquino, C.L.E.; Balela, M.D.L. Photo-Fenton Degradation of Methyl Orange Using Hematite (α -Fe₂O₃) of Various Morphologies. *Mater. Today Proc.* **2020**, *22*, 248–254. [[CrossRef](#)]
5. Nyankson, E.; Kumar, R.V. Removal of Water-Soluble Dyes and Pharmaceutical Wastes by Combining the Photocatalytic Properties of Ag₃PO₄ with the Adsorption Properties of Halloysite Nanotubes. *Mater. Today Adv.* **2019**, *4*, 100025. [[CrossRef](#)]
6. Alharthi, F.A.; Al-Zaqri, N.; El Marghany, A.; Alghamdi, A.A.; Alorabi, A.Q.; Baghdadi, N.; AL-Shehri, H.S.; Wahab, R.; Ahmad, N. Synthesis of Nanocauliflower ZnO Photocatalyst by Potato Waste and Its Photocatalytic Efficiency against Dye. *J. Mater. Sci. Mater. Electron.* **2020**, *31*, 11538–11547. [[CrossRef](#)]
7. Natarajan, S.; Bajaj, H.C.; Tayade, R.J. Recent Advances Based on the Synergetic Effect of Adsorption for Removal of Dyes from Waste Water Using Photocatalytic Process. *J. Environ. Sci.* **2018**, *65*, 201–222. [[CrossRef](#)] [[PubMed](#)]
8. Kumar, S.; Kaushik, R.D.; Purohit, L.P. Novel ZnO Tetrapod-Reduced Graphene Oxide Nanocomposites for Enhanced Photocatalytic Degradation of Phenolic Compounds and MB Dye. *J. Mol. Liq.* **2021**, *327*, 114814. [[CrossRef](#)]
9. Hasanpour, M.; Hatami, M. Photocatalytic Performance of Aerogels for Organic Dyes Removal from Wastewaters: Review Study. *J. Mol. Liq.* **2020**, *309*, 113094. [[CrossRef](#)]
10. Nawaz, A.; Khan, A.; Ali, N.; Ali, N.; Bilal, M. Fabrication and Characterization of New Ternary Ferrites-Chitosan Nanocomposite for Solar-Light Driven Photocatalytic Degradation of a Model Textile Dye. *Environ. Technol. Innov.* **2020**, *20*, 101079. [[CrossRef](#)]
11. Berradi, M.; Hsissou, R.; Khudhair, M.; Assouag, M.; Cherkaoui, O.; El Bachiri, A.; El Harfi, A. Textile Finishing Dyes and Their Impact on Aquatic Environs. *Heliyon* **2019**, *5*, e02711. [[CrossRef](#)] [[PubMed](#)]
12. Alakhras, F.; Alhajri, E.; Haounati, R.; Ouachtak, H.; Addi, A.A.; Saleh, T.A. A Comparative Study of Photocatalytic Degradation of Rhodamine B Using Natural-Based Zeolite Composites. *Surf. Interfaces* **2020**, *20*, 100611. [[CrossRef](#)]
13. Fu, F.; Wang, Q. Removal of Heavy Metal Ions from Wastewaters: A Review. *J. Environ. Manag.* **2011**, *92*, 407–418. [[CrossRef](#)] [[PubMed](#)]
14. Moosavi, S.; Lai, C.W.; Gan, S.; Zamiri, G.; Akbarzadeh Pivezhani, O.; Johan, M.R. Application of Efficient Magnetic Particles and Activated Carbon for Dye Removal from Wastewater. *ACS Omega* **2020**, *5*, 20684–20697. [[CrossRef](#)] [[PubMed](#)]
15. De Gisi, S.; Lofrano, G.; Grassi, M.; Notarnicola, M. Characteristics and Adsorption Capacities of Low-Cost Sorbents for Wastewater Treatment: A Review. *Sustain. Mater. Technol.* **2016**, *9*, 10–40. [[CrossRef](#)]
16. Mahdi, A.E.; Ali, N.S.; Kalash, K.R.; Salih, I.K.; Abdulrahman, M.A.; Albayati, T.M. Investigation of Equilibrium, Isotherm, and Mechanism for the Efficient Removal of 3-Nitroaniline Dye from Wastewater Using Mesoporous Material MCM-48. *Prog. Color Color Coat.* **2023**, *16*, 387–398.

17. Raffiean, S.; Mirzadeh, H.; Mahdavi, H.; Masoumi, M.E. A Review on Nanocomposite Hydrogels and Their Biomedical Applications. *Sci. Eng. Compos. Mater.* **2019**, *26*, 154–174. [[CrossRef](#)]
18. Chronopoulou, L.; Binaymotlagh, R.; Cerra, S.; Hajareh Haghighi, F.; Di Domenico, E.G.; Sivori, F.; Fratoddi, I.; Mignardi, S.; Palocci, C. Preparation of Hydrogel Composites Using a Sustainable Approach for In Situ Silver Nanoparticles Formation. *Materials* **2023**, *16*, 2134. [[CrossRef](#)] [[PubMed](#)]
19. Binaymotlagh, R.; Hajareh Haghighi, F.; Di Domenico, E.G.; Sivori, F.; Truglio, M.; Del Giudice, A.; Fratoddi, I.; Chronopoulou, L.; Palocci, C. Biosynthesis of Peptide Hydrogel–Titania Nanoparticle Composites with Antibacterial Properties. *Gels* **2023**, *9*, 940. [[CrossRef](#)]
20. Fortunato, A.; Mba, M. A Peptide-Based Hydrogel for Adsorption of Dyes and Pharmaceuticals in Water Remediation. *Gels* **2022**, *8*, 672. [[CrossRef](#)]
21. Veloso, S.R.S.; Ferreira, P.M.T.; Martins, J.A.; Coutinho, P.J.G.; Castanheira, E.M.S. Magnetogels: Prospects and Main Challenges in Biomedical Applications. *Pharmaceutics* **2018**, *10*, 145. [[CrossRef](#)] [[PubMed](#)]
22. de Melo, F.M.; Grasseschi, D.; Brandão, B.B.N.S.; Fu, Y.; Toma, H.E. Superparamagnetic Maghemite-Based CdTe Quantum Dots as Efficient Hybrid Nanoprobes for Water-Bath Magnetic Particle Inspection. *ACS Appl. Nano Mater.* **2018**, *1*, 2858–2868. [[CrossRef](#)]
23. Hajareh Haghighi, F.; Binaymotlagh, R.; Chronopoulou, L.; Cerra, S.; Marrani, A.G.; Amato, F.; Palocci, C.; Fratoddi, I. Self-Assembling Peptide-Based Magnetogels for the Removal of Heavy Metals from Water. *Gels* **2023**, *9*, 621. [[CrossRef](#)] [[PubMed](#)]
24. Chronopoulou, L.; Lorenzoni, S.; Masci, G.; Dentini, M.; Togna, A.R.; Togna, G.; Bordi, F.; Palocci, C. Lipase-Supported Synthesis of Peptidic Hydrogels. *Soft Matter* **2010**, *6*, 2525–2532. [[CrossRef](#)]
25. Sáenz-Trevizo, A.; Pizá-Ruiz, P.; Chávez-Flores, D.; Ogaz-Parada, J.; Amézaga-Madrid, P.; Vega-Ríos, A.; Miki-Yoshida, M. On the Discoloration of Methylene Blue by Visible Light. *J. Fluoresc.* **2019**, *29*, 15–25. [[CrossRef](#)] [[PubMed](#)]
26. Purcar, V.; Donescu, D.; Petcu, C.; Vasilescu, M. Nanostructured Hybrid Systems with Rhodamine 6G. *J. Dispers. Sci. Technol.* **2008**, *29*, 1233–1239. [[CrossRef](#)]
27. Ruiz, C.; Vera, M.; Rivas, B.L.; Sánchez, S.A.; Urbano, B.F. Magnetic methacrylated gelatin-g-polyelectrolyte for methylene blue sorption. *RSC Adv.* **2020**, *10*, 43799–43810. [[CrossRef](#)] [[PubMed](#)]
28. Yao, G.; Bi, W.; Liu, H. pH-responsive magnetic graphene oxide/poly(NVI-co-AA) hydrogel as an easily recyclable adsorbent for cationic and anionic dyes. *Colloids Surf. A Physicochem. Eng. Asp.* **2020**, *588*, 124393. [[CrossRef](#)]
29. Gang, F.; Jiang, L.; Xiao, Y.; Zhang, J.; Sun, X. Multi-functional magnetic hydrogel: Design strategies and applications. *Nano Select* **2021**, *2*, 2291–2307. [[CrossRef](#)]
30. Veloso, S.R.S.; Andrade, R.G.D.; Castanheira, E.M.S. Review on the advancements of magnetic gels: Towards multifunctional magnetic liposome-hydrogel composites for biomedical applications. *Adv. Colloid Interface Sci.* **2021**, *288*, 102351. [[CrossRef](#)]
31. Van Berkum, S.; Biewenga, P.D.; Verkleij, S.P.; Van Zon, J.B.A.; Boere, K.W.M.; Pal, A.; Philipse, A.P.; Ern , B.H. Swelling Enhanced Remanent Magnetization of Hydrogels Cross-Linked with Magnetic Nanoparticles. *Langmuir* **2014**, *31*, 442–450. [[CrossRef](#)] [[PubMed](#)]
32. Saadli, M.; Braunmiller, D.L.; Mourran, A.; Crassous, J.J. Thermally and Magnetically Programmable Hydrogel Microactuators. *Small* **2023**, *19*, 2207035. [[CrossRef](#)] [[PubMed](#)]
33. Nagireddy, N.R.; Yallapu, M.M.; Kokkarachedu, V.; Sakey, R.; Kanikireddy, V.; Pattayil Alias, J.; Konduru, M.R. Preparation and Characterization of Magnetic Nanoparticles Embedded in Hydrogels for Protein Purification and Metal Extraction. *J. Polym. Res.* **2011**, *18*, 2285–2294. [[CrossRef](#)]
34. Sharma, G.; Garc a-Pe as, A.; Verma, Y.; Kumar, A.; Dhiman, P.; Stadler, F.J. Tailoring Homogeneous Hydrogel Nanospheres by Facile Ultra-Sonication Assisted Cross-Linked Copolymerization for Rhodamine B Dye Adsorption. *Gels* **2023**, *9*, 770. [[CrossRef](#)] [[PubMed](#)]
35. Rana, H.; Anamika, A.; Sareen, D.; Goswami, S. Nanocellulose-Based Ecofriendly Nanocomposite for Effective wastewater Remediation: A study on its process optimization, improved swelling, adsorption, and thermal and mechanical behavior. *ACS Omega* **2024**, *9*, 8904–8922. [[CrossRef](#)]
36. Gao, H.; Jiang, J.; Huang, Y.; Wang, H.; Sun, J.; Jin, Z.; Wang, J.; Zhang, J. Synthesis of hydrogels for adsorption of anionic and cationic dyes in water: Ionic liquid as a crosslinking agent. *SN Appl. Sci.* **2022**, *4*, 118. [[CrossRef](#)]
37. Chen, T.; Liu, H.; Gao, J.; Hu, G.; Zhao, Y.; Tang, X.; Han, X. Efficient removal of methylene blue by Bio-Based sodium Alginate/Lignin composite hydrogel beads. *Polymers* **2022**, *14*, 2917. [[CrossRef](#)] [[PubMed](#)]
38. Wang, W.; Bai, H.; Zhao, Y.; Kang, S.; Yi, H.; Zhang, T.; Song, S. Synthesis of chitosan cross-linked 3D network-structured hydrogel for methylene blue removal. *Int. J. Biol. Macromol.* **2019**, *141*, 98–107. [[CrossRef](#)] [[PubMed](#)]
39. Wang, J.; Meng, X.; Yuan, Z.; Tian, Y.; Bai, Y.; Jin, Z. Acrylated Composite Hydrogel Preparation and Adsorption Kinetics of Methylene Blue. *Molecules* **2017**, *22*, 1824. [[CrossRef](#)]
40. Li, Y.; Liu, L.; Huang, W.; Xie, J.; Song, Z.; Guo, S.; Wang, E. Preparation of peanut shell cellulose Double-Network hydrogel and its adsorption capacity for methylene blue. *J. Renew. Mater.* **2023**, *11*, 3001–3023. [[CrossRef](#)]
41. Godiya, C.B.; Xiao, Y.; Lu, X. Amine Functionalized Sodium Alginate Hydrogel for Efficient and Rapid Removal of Methyl Blue in Water. *Int. J. Biol. Macromol.* **2020**, *144*, 671–681. [[CrossRef](#)] [[PubMed](#)]
42. Fern ndez-P rez, A.; Marb n, G. Visible Light Spectroscopic Analysis of Methylene Blue in Water; What Comes after Dimer? *ACS Omega* **2020**, *5*, 29801–29815. [[CrossRef](#)] [[PubMed](#)]

43. Li, S.; Liu, X.; Huang, W.; Li, W.; Xia, X.; Yan, S.; Yu, J. Magnetically assisted removal and separation of cationic dyes from aqueous solution by magnetic nanocomposite hydrogels. *Polym. Adv. Technol.* **2011**, *22*, 2439–2447. [[CrossRef](#)]
44. Ludeña, M.A.; Meza, F.d.L.; Huamán, R.I.; Lechuga, A.M.; Valderrama, A.C. Preparation and Characterization of Fe₃O₄/Poly(HEMA-co-IA) Magnetic Hydrogels for Removal of Methylene Blue from Aqueous Solution. *Gels* **2024**, *10*, 15. [[CrossRef](#)]
45. Yuan, Z.; Wang, Y.; Han, X.; Chen, D. The adsorption behaviors of the multiple stimulus-responsive poly(ethylene glycol)-based hydrogels for removal of RhB dye. *J. Appl. Polym. Sci.* **2015**, *132*, 42244. [[CrossRef](#)]

Disclaimer/Publisher’s Note: The statements, opinions and data contained in all publications are solely those of the individual author(s) and contributor(s) and not of MDPI and/or the editor(s). MDPI and/or the editor(s) disclaim responsibility for any injury to people or property resulting from any ideas, methods, instructions or products referred to in the content.